This article has been accepted for publication in a future issue of this journal, but has not been fully edited. Content may change prior to final publication. Citation information: DOI 10.1109/TUFFC.2018.2875781, IEEE Transactions on Ultrasonics, Ferroelectrics, and Frequency Control

Establishing the limits of validity of the superposition of experimental and analytical ultrasonic responses for simulating imaging data

Harry A. Bloxham, Alexander Velichko, Paul D. Wilcox

***Abstract*—The superposition of experimental and analytical data is useful for simulating ultrasonic images of defects in samples containing high levels of coherent structural noise. This technique assumes that the superposition of the response of a defect in a homogeneous medium with that of a heterogeneous, defect-free medium is identical to the response of the same defect embedded in the heterogeneous medium. This implies a single-scattering process. Previous experimental work demonstrated successful use of the technique, but only over a limited range of defect Signal to Noise Ratios (SNRs). However, there was a concern that it might not remain valid at low SNR due to, for example, multiple-scattering effects. This paper shows that this technique provides accurate results over the full range of SNRs of defects where the defect is discernible from image noise. The technique is therefore suitable for simulating any inspection where ultrasonic imaging is an appropriate method of NDE.**

I. Introduction

For a Non-Destructive Evaluation (NDE) inspection to be effective in industry, the limits of what can be detected must be known to ensure it is capable of identifying all defects considered unsafe for the item in question. These limits are reached when the defect response becomes indistinguishable from the noise in the image. Many common engineering materials exhibit large levels of coherent noise when imaged ultrasonically due to inhomogeneities. In metals, this noise is caused by discontinuity in acoustic impedance at grain boundaries [1], [2] and becomes significant when the grain size is of the order of the wavelength of the ultrasound [3].

One common method of evaluating the limits of the inspection is with the use of Probability Of Detection (POD) curves [4]. Traditionally, these curves have been calculated using large numbers of experimental results requiring many samples and trained technicians to perform the inspections, all at a great cost [5]. There is a trend towards using model-based and model-assisted POD (MAPOD) curves to reduce this cost [6], however, this method requires simulations with a high degree of accuracy. While the principles behind simulating ultrasonic data and their resultant images has been known for several decades [7], [8], accurately simulating all sources of noise in real inspections proves difficult to achieve using analytical methods. The superposition of experimental and analytical data has been recently been used in guided wave applications [9]. In addition, previous work by the authors [10] has shown that this technique can also be applied to phased arrays to provide accurate simulations of ultrasonic imaging data in scenarios where coherent noise, from both geometrical features and material grains, make fully analytical simulations difficult. However, this was only validated for defects with moderate to high Signal-to-Noise Ratios (SNRs). To realise this technique's full potential, it is necessary to demonstrate its validity on defects with low SNRs to give confidence in its use as a method of performing a limits of detectability study for an inspection while requiring only a very limited set of experimental data.

The work in [10] makes the assumption that the superposition of the response in a defect-free sample with an analytically calculated defect response is identical to the response of the same sample containing the same defect. This was empirically shown to be a valid assumption for the scenario described but this may not be true for all possible cases. In reality, the addition of a defect will include shadowing effects on grains in the region behind the defect which are not accounted for in the model. Determining if this difference has a statistically significant effect on the image in this region is one of the aims of this paper. The other principal aim of this work is to validate the accuracy of image amplitudes for defects with a low SNR when they are

This work was funded by a UK Engineering and Physical Sciences Research Council industrial CASE award supported by BAE Systems Marine Ltd. (grant number 14220026).

The authors are with the Department of Mechanical Engineering, University of Bristol, Bristol, BS8 1TR, UK (e-mail:h.bloxham@bristol.ac.uk).

This article has been accepted for publication in a future issue of this journal, but has not been fully edited. Content may change prior to final publication. Citation information: DOI 10.1109/TUFFC.2018.2875781, IEEE Transactions on Ultrasonics, Ferroelectrics, and Frequency Control

on the limit of detectability.

II. Method

To achieve the aims of this paper, it is necessary to examine the differences between the ultrasonic response of two samples, one with a defect present and one without, but both with identical grain structure. An analytically calculated defect response can then be summed with the response from a defect-free sample and this compared to the response from the sample with the defect present. This differs from the previous work by the authors in that both of these responses being compared come from samples with identical grain structure, and therefore coherent noise.

It is theoretically possible to collect these results experimentally by taking measurements both before and after a defect is machined into the sample. However, this proves extremely challenging due to difficulties in maintaining the precise array alignment and environmental variables between measurements. Changes to the grain structure local to the defect caused by the machining process can also introduce errors. Because of this, Finite Element (FE) techniques have been used to simulate these responses. Much work has been done on the FE modelling of ultrasonic propagation and it has been shown to give strong agreement with experimental results [11]–[13] including with heterogeneous materials by modelling individual grains within the material and applying the relevant anisotropic material properties to each grain [14].

A. Grain modelling

In order to accurately model the scattering caused by the micro-structure of a material, each grain must be described individually within the model and its orientation defined. The use of Voronoi diagrams [15] is becoming a common technique used to simulate the grain structure of a material [16], [17] and has previously been used to study the ultrasonic scattering of heterogeneous materials [14], [18]. To simulate a grain structure using this method, first a uniform grid of nodes is created. Each node is then shifted a random amount according to a zero mean Gaussian distribution, with a standard deviation equal to the spread parameter, in each dimension and a Voronoi diagram based on these nodes is made. This Voronoi diagram consists of a series of convex polygons, one surrounding each node, the boundary of which defines the region of the diagram which is closest to the node it encloses, an example can be seen in figure 1A. The spacing of the initial uniform nodes will determine the mean grain size in the final structure and their variation in size is linked to the Gaussian distribution used to displace them. Each grain is then assigned a random orientation in 3D and the appropriate material properties are specified.

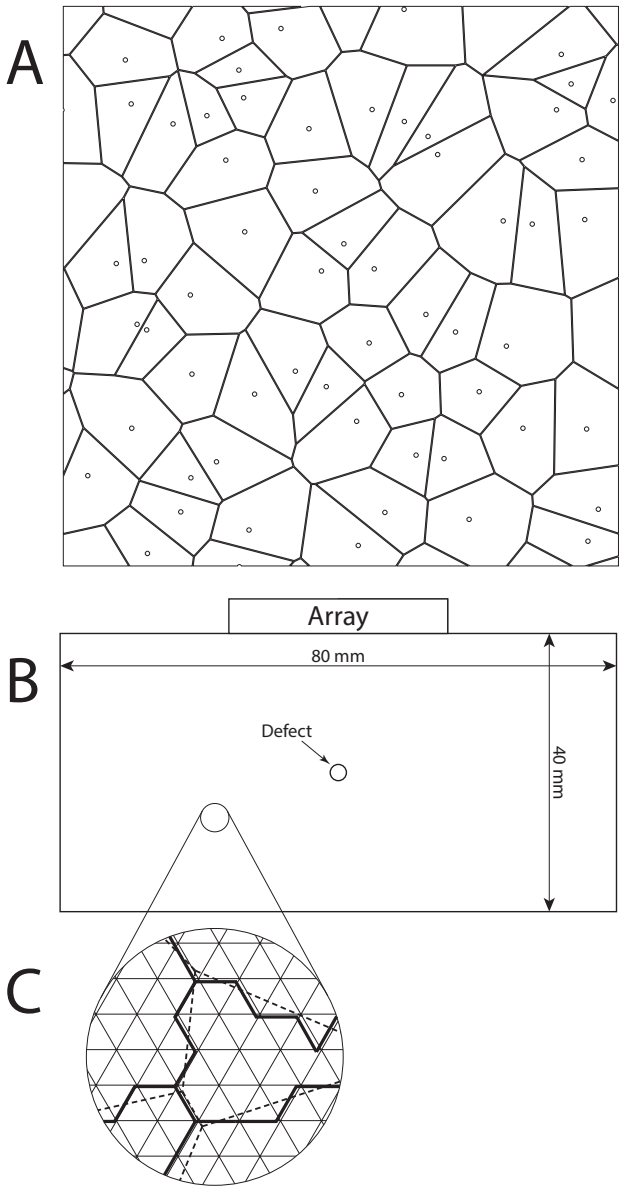

Fig. 1. Example of Voronoi diagram to represent grain structure with seed nodes indicated by open circles (A), the FE model geometry (B) and and example of the staircasing effect caused by a structured mesh (C). The faint lines represent the model element boundaries, the dashed lines represent the material grain boundary defined by the Voronoi diagram and the bold lines show the staircased grain boundaries used in the model.

B. Finite element modelling

Recent advances in computing hardware have meant that FE techniques have become a more viable method of simulating ultrasonic imaging data due to reduced computation time. The most significant advance has been in the utilisation of Graphics Processing Units

This article has been accepted for publication in a future issue of this journal, but has not been fully edited. Content may change prior to final publication. Citation information: DOI 10.1109/TUFFC.2018.2875781, IEEE Transactions on Ultrasonics, Ferroelectrics, and Frequency Control

(GPUs) which have been shown to reduce the processing time by 1-2 orders of magnitude [19]. An open-source software package called Pogo (www.pogo-fea.com) which implements this technology has been used for the simulations described in this paper.

Using Pogo, both structured and unstructured meshes are available, each with their own benefits and disadvantages. Structured meshes fit the model structure to a pre-defined arrangement of elements, usually forming a regular grid, whereas unstructured meshes fit the elements to the geometery that is being simulated. The benefits of an unstructured mesh are that it can very closely match the geometry of the structure; however, it can leave the mesh with undesirably small elements which limits the maximum stable time step of the solver and causes the whole model to run more slowly. Structured meshes do not have this problem as element size is fixed. This however means that the geometry of the model (here, the boundaries of the grains) must be modified to match the boundaries of the elements in the mesh. For this work, a structured mesh has been used for efficiency, with the element size chosen to be sufficiently small such that any modification to the grain boundaries has a negligible effect on an ultrasonic wave front at the frequencies used in this work. The effect a structured mesh has on the grain boundaries of the model can be seen in figure 1C (note that the element size has been enlarged relative to the grain size to exaggerate the effect). This stair-casing's effect on wave propagation from a defect was studied by Drozdz [20] and was found to have an insignificant effect at half the mesh density of that used in the work presented in this paper. Additionally, the effect at grain boundaries will be less significant than at a defect due to the less coherent nature of these signals caused by multiple scattering.

For this work, a 2-dimensional models of a $40\,\mathrm{mm}$ deep sample with a defect at a depth $20\,\mathrm{mm}$ was used, as seen in figure 1B. The mean grain size was $100\,\mu\mathrm{m}$ with a spread parameter of $200\,\mu\mathrm{m}$. The orthotropic material properties used for each grain are given in Table I.

TABLE I
MATERIAL PROPERTIES

Property	Value
E_{11}	$168.6\,\mathrm{GPa}$
E_{12}	$121.4\,\mathrm{GPa}$
E_{44}	$75.4\,\mathrm{GPa}$
ρ	$8960\,\mathrm{kg/m^3}$

The FE model is used to simulate the process of acquiring a Full Matrix Capture (FMC) data set. To do this, the vertical displacement at nodes on the top edge of the model, corresponding to the location of an array's transducer elements, are monitored while a vertical force is applied to the nodes representing a single element of the array to excite a wideband ultrasonic pulse. The vertical displacements of the nodes representing each element in the array are summed to give the response of that element. This process is repeated for all elements to create the response from all transmit-receive element pairs. The input signal used for this paper was a Gaussian windowed, single cycle, $2.5\,\mathrm{MHz}$ pulse. The element edge length was $30\,\mu\mathrm{m}$, approximately equivalent to 60 elements per wavelength at the centre frequency in the equivalent homogeneous material.

For each defect investigated, the model was run using 30 different realisations of random grain structures and for each grain structure, the model was run twice, once with the defect and once without. These results were used in place of experimental results as 'truths' to which the superposition technique results can be compared.

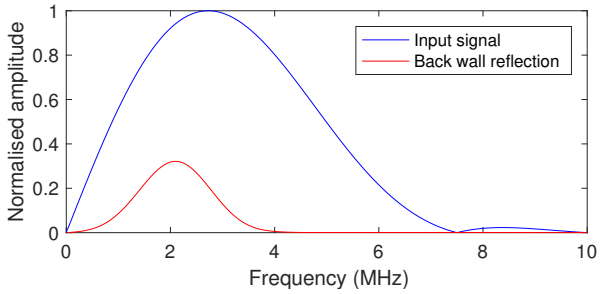

Fig. 2. Frequency spectra of the input signal for the analytical model and the first back wall reflection predicted by the model.

A wideband input signal, formed of a single cycle toneburst, was used for all the simulations in this paper to allow for a single model run to provide results for a wide range of frequencies by the use of appropriate filters. Due to attenuation increasing with frequency however, much of the higher end of the spectrum is attenuated to a level comparable with the noise meaning any images formed using data filtered at these higher frequencies are likely to be dominated by noise. This can be seen in figure 2 which shows that despite there being significant frequency content above 5 MHz in the input signal, there is almost none in the first back wall reflection. The frequency range considered in this paper is therefore representative of the usable frequencies for the given geometry and material properties and is not limited by the bandwidth of the input signal.

This article has been accepted for publication in a future issue of this journal, but has not been fully edited. Content may change prior to final publication. Citation information: DOI 10.1109/TUFFC.2018.2875781, IEEE Transactions on Ultrasonics, Ferroelectrics, and Frequency Control

C. Superposition of data sets

The method used to combine an analytical defect with a defect-free data set is described in detail in [10] and termed the superposition technique. A summary is provided here for reference. For this technique, some parameters must be determined by independent measurements. These are the specimen's depth, d, the homogenised speed of sound, c and frequency-dependant attenuation coefficient, α.

Next, a defect-free data set is obtained either experimentally or, in the case of the current paper, via FE simulation. The back wall signal from the defect-free data set is back-propagated to give the input signal for an analytical ray-based model calculated using:

$$U_{input}(\omega) = B_1(\omega)e^{2d\alpha(\omega)}e^{-2i\omega d/c}, \qquad (1)$$

where U_{input} is the input signal, ω is the angular frequency and B_1 is the frequency spectrum of the first back wall reflection.

The analytical ray-based model is then used to simulate the defect response and back wall shadowing effects that would occur if the defect was present in the defect-free data set. This response is calculated using the scattering matrix for the given defect. This matrix describes the relationship between the amplitude and phase of the scattered wave from the defect as a function of incident angle, scattering angle and frequency. The superposition of these two data sets is intended to give an accurate representation of the ultrasonic image that would be obtained if the defect was present in the sample.

D. Determination of ultrasonic velocity and attenuation

To be able to simulate the defect and shadowing responses for use with the superposition technique, the attenuation and longitudinal wave velocity of the material must be calculated. This can be done using the first and second back wall reflections from the sum of all transmit-receive pairs from the FMC data for the defect-free case as seen in figure 3A. A simple time of flight calculation based on the difference in arrival times of these two reflections gives the wave velocity. To calculate the attenuation, the frequency spectra of these two reflections are required, as shown in figure 3B. Ignoring diffraction, the attenuation can then be calculated using:

$$\alpha(\omega) = \frac{1}{2d}\ln\left|\frac{B_1(\omega)}{B_2(\omega)}\right|, \qquad (2)$$

where B_2 is the frequency spectrum of the second back wall reflection. This will only give reliable values for α at frequencies where both spectra have amplitudes sufficient to dominate over the noise response. A cubic fit to the measured $\alpha(\omega)$ is then used over the range of reliable frequencies for use in the simulations. By necessity, the attenuation coefficient for frequencies outside of this range must be extrapolated; the results of this can be seen in figure 3C.

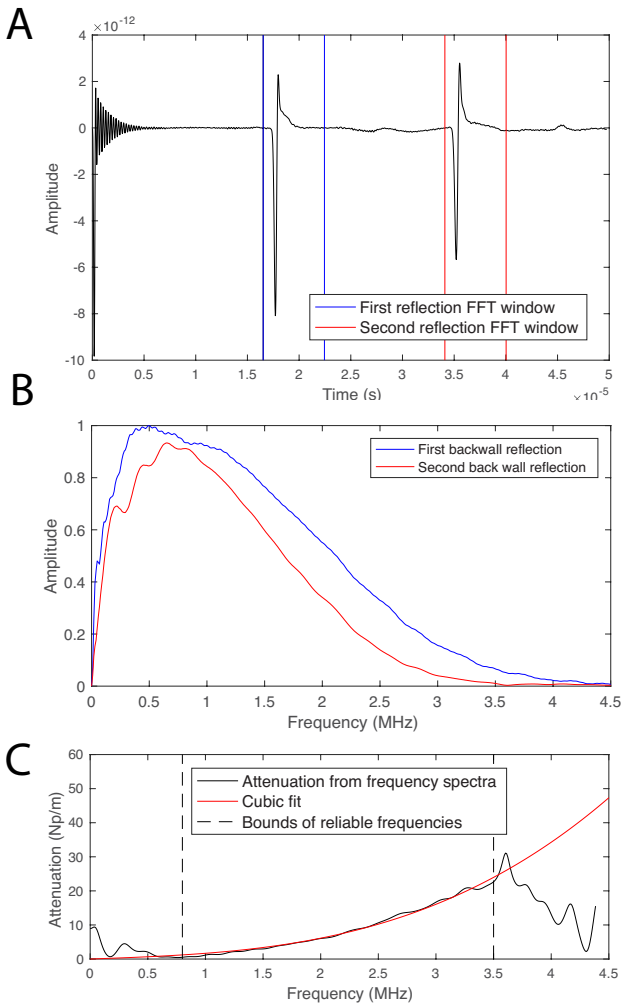

Fig. 3. Sum of the time traces from all transmit-receive pairs of the array averaged over multiple realisations and the relevant windows for the Fourier transform for the first two back wall reflections (A), the normalised frequency spectra of these reflections (B) and the frequency dependant attenuation coefficient calculated from these spectra (C).

III. Results

Figure 4 shows images created using the Total Focusing Method (TFM). In the first column, the data is filtered with a 2.5 MHz centre frequency Gaussian filter with a half bandwidth of 2.5MHz before imaging. In the other columns the data is filtered with 0.5MHz half bandwidth Gaussian filters at the centre frequencies

This article has been accepted for publication in a future issue of this journal, but has not been fully edited. Content may change prior to final publication. Citation information: DOI 10.1109/TUFFC.2018.2875781, IEEE Transactions on Ultrasonics, Ferroelectrics, and Frequency Control

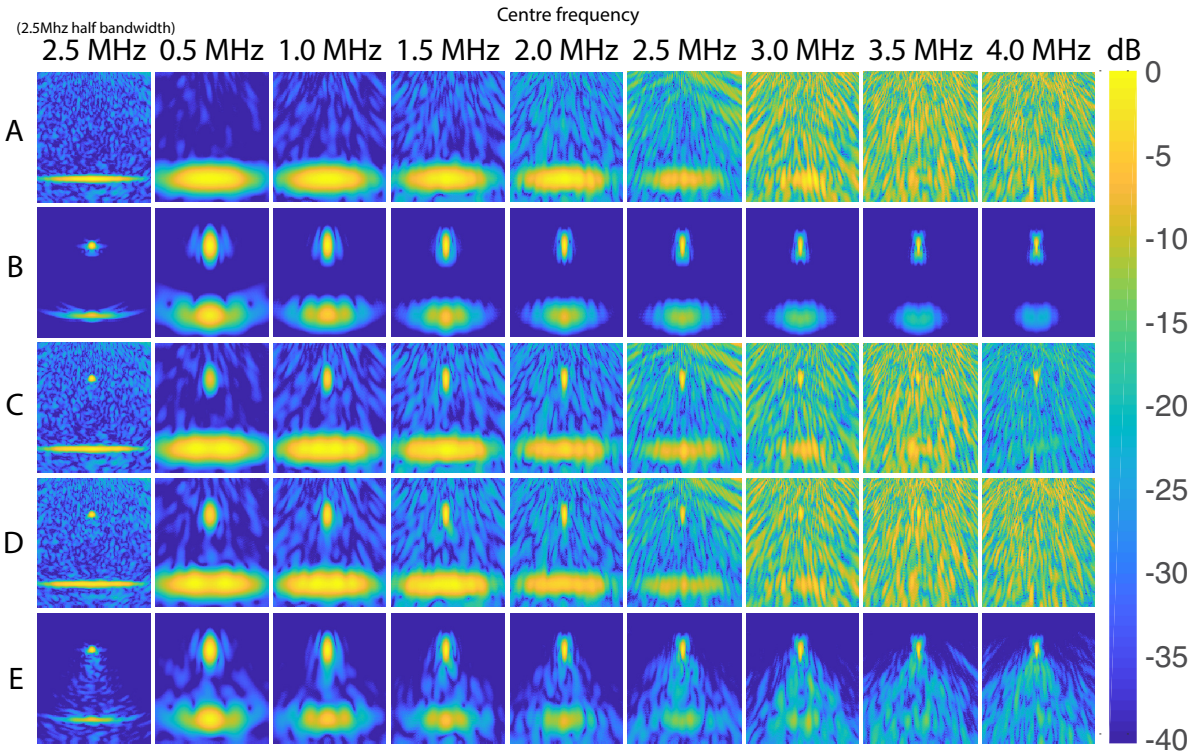

Fig. 4. TFM images at various frequencies of FE defect-free case (A), the analytically calculated defect response and shadowing effects (B), the superposition of A & B (C), FE model with defect present (D) and the difference between A & D (E) . All images are filtered at the labelled centre frequency with a half bandwidth of 0.5 MHz except the 2.5 MHz full bandwidth column which has a 2.5 MHz half bandwidth.

stated. Row A shows images from one realisation of the defect-free case from the FE model, row B shows the analytically calculated defect and shadowing responses for a 2 mm side-drilled hole, row C shows the superposition of the results from rows A & B, row D shows the FE-model with a 2 mm side-drilled hole for the same realisation of grains as in row A. Finally row E shows the difference between rows A & D. The superposition model gives very accurate results when filtered over a wide bandwidth, as typical in industry. This can be seen by comparing figures 4C and 4D in the first column. An assumption of the superposition technique is that the defect response and shadowing effect calculated using a scattering matrix are identical to the change in the image caused by introducing a defect, i.e. that rows B & E are identical. From figure 4E, it can be seen that this is approximately true when the noise level is low but ceases to be the case as the frequency and noise level increase. The results in figures 4B & E show good agreement for the strongest features, the defect and back wall shadowing. However, there is a large area of low amplitude speckle below the defect. This is caused by the defect shadowing a region of grains from the array which is not accounted for in the analytical model used in the superposition technique. This means that the speckle behind the defect predicted by the superposition technique is different to the speckle observed in the full FE model. However, for practical purposes it can only be considered an error if it alters the speckle statistics in this region.

IV. Discussion

A. Accuracy of image amplitude predictions

To gain a more quantitative understanding of the limit at which the superposition technique is valid, the results were examined when filtered over a narrower bandwidth of 0.5MHz for 30 different realisations of noise. This was done for two defect types, straight cracks and side drilled holes for a variety of sizes.

Figure 5 shows the bounds of one standard deviation either side of the mean of the image amplitude for various features. These are; the maximum amplitude of the defect; the mean amplitude along a line 10 mm long, parallel to the back wall and located in the centre of the back wall; and the RMS noise measured in the region between the defect and back wall where there is the greatest discrepancy between the two models as seen in figure 4E. This was done for the superposition model and the FE model as a function of frequency for a range of defects. It is evident in figure 5 that the

This article has been accepted for publication in a future issue of this journal, but has not been fully edited. Content may change prior to final publication. Citation information: DOI 10.1109/TUFFC.2018.2875781, IEEE Transactions on Ultrasonics, Ferroelectrics, and Frequency Control

TABLE II
WIDE BANDWIDTH IMAGE AMPLITUDE ERRORS.

Error in:	Defect	RMS noise	Back wall
0.5 mm hole	-0.02 dB	-0.07 dB	-0.15 dB
2.0 mm hole	0.20 dB	0.15 dB	-0.20 dB
5.0 mm hole	0.05 dB	2.23 dB	-0.88 dB
2.0 mm crack	0.33 dB	0.52 dB	-0.19 dB
5.0 mm crack	0.34 dB	1.40 dB	0.06 dB

superposition technique provides an accurate prediction for defect image amplitude and RMS noise level for all defects simulated. Additionally, back wall shadowing effects are, in general, reproduced accurately but some discrepancies are seen for some of the larger defects (2 mm hole, 5 mm crack & hole) over a limited frequency range at the lower end of the spectrum. Difficulties in simulating the shadowing effects from larger defect were also encountered in [10] and are thought to be due to the extreme sensitivity of the high levels of destructive interference required to produce the shadowing effects associated with these larger defects. At the upper end of the frequency spectrum, the superposition technique shows a significantly wider spread of defect image amplitudes between different realisations of noise.

To see how these discrepancies translate into images filtered at a more realistic half-bandwidth, table II shows the mean difference in image amplitudes between the FE model and superposition model when the results are filtered with a 2 MHz centre frequency and 2 MHz half-bandwidth.

B. Identifying the frequency range of interest

While figure 5 shows that the superposition model ceases to be a reliable approximation to the true response as frequency increases, the aim of the paper is to determine whether the technique is applicable over a practically useful frequency range, not over all frequencies. For this reason it is necessary to define the frequency range of interest and this is done by considering the mean SNR of the defects. Once the SNR drops, it becomes impossible to achieve an adequate probability of detection without incurring a high number of false alarms.

The SNR, calculated as the ratio between the maximum amplitude of the target and the RMS noise value, was evaluated for all of the defects and for the back wall in the defect-free case. This was calculated from the FE data and the results are shown in figure 6. It is common practice to set a threshold amplitude, over which any pixel in the image can be considered a defect. For this paper, the threshold level has been set at 12.5 dB above

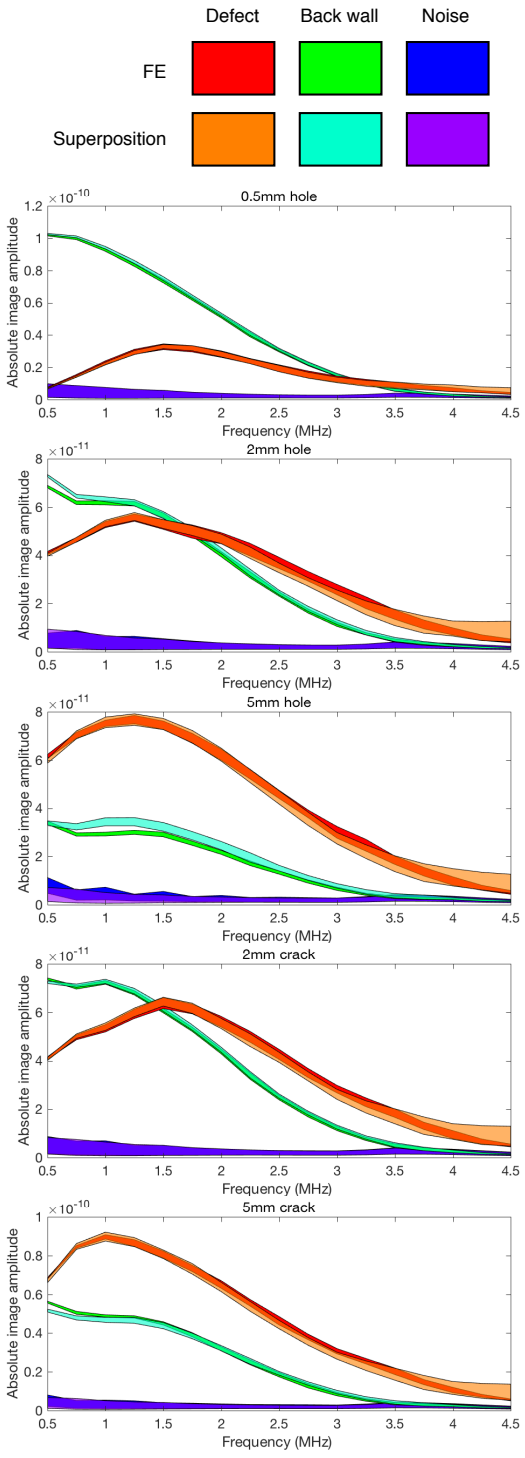

Fig. 5. Comparisons between FE and superposition model images amplitudes measured at the defect and back wall and the RMS noise value in the region behind the defect. The lines are centred on the mean over the 30 realisations of noise with the line width representing two standard deviations. The filter half-bandwidth is 0.5 MHz.

This article has been accepted for publication in a future issue of this journal, but has not been fully edited. Content may change prior to final publication. Citation information: DOI 10.1109/TUFFC.2018.2875781, IEEE Transactions on Ultrasonics, Ferroelectrics, and Frequency Control

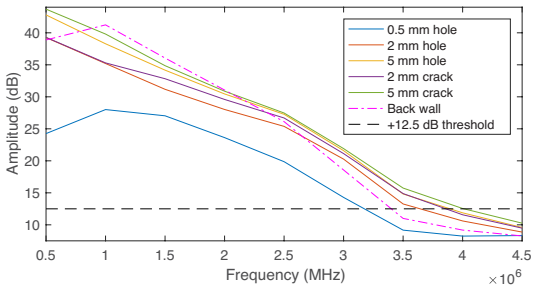

Fig. 6. SNR of defects and back wall. The filter half-bandwidth is 0.5 MHz.

the RMS noise value and this can also be seen in figure 6. This has been calculated to give a false call ratio of 1 in 1000 for the given image size and assuming the image pixel amplitude due to speckle follows a Rayleigh distribution.

The results in figure 6 show that the SNR falls below the threshold value at between approximately 3.2 and 4.0 MHz for the various defects and back wall. These frequencies can be considered as the limits of detectability for the given defect as at higher frequencies, the inspection is unable to detect the defect without exceeding the acceptable false call ratio criterion. These frequencies also correlate approximately with where the back wall image amplitudes become comparable with the RMS noise amplitude seen in figure 5. Below these frequencies, the superposition technique provides results that are on average accurate to within 1 dB. However, the limits presented here are only valid for the given geometry and will be affected by any change in the defect depth in the sample.

Above these frequencies, figure 5 shows that there is a significantly increased variation in predicted image amplitudes. The superposition technique is believed to fail at higher frequencies because it becomes impossible to reliably extract an input signal from the back wall to use in the analytical defect model, rather than a failure in the superposition assumption itself. This is because the back wall amplitude falls within the expected range of noise amplitude and so any extracted input signal will be dominated by noise.

C. Defects at the limit of detectability

While figure 5 shows that the superposition technique provides accurate results for the defects presented, the defects considered are all sufficiently large that they are significantly over the threshold value when imaged at a suitable frequency.

To further investigate the accuracy of the superposition technique for defects with low SNR, its results were compared to the FE model for the smallest hole which could be detected in a TFM image for the inspection geometry and material properties used for the previous defects. To determine the size of this hole, the sensitivity to defects of the inspection was maximised by use of an optimised standard Gaussian filter (defined as where the half-bandwidth is equal to the centre frequency). The superposition technique was then used to estimate the smallest hole diameter which would produce an image amplitude just greater than the +12.5 dB threshold and this was calculated to be 0.14 mm.

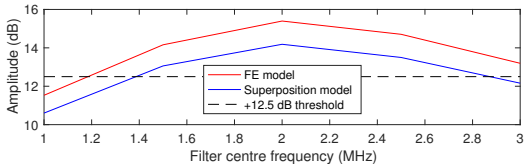

Fig. 7. SNR of a 0.14 mm hole simulated using the FE model and superposition technique. The filter is a standard Gaussian filter with half bandwidth equal to the centre frequency.

Figure 7 shows the SNR of a 0.14 mm hole simulated using both the FE model and superposition technique at various filter centre frequencies using standard Gaussian filters. These results show that the optimum standard filter predicted by the superposition model is one with a centre frequency of 2 MHz and that the 'true' FE model predicts the same value; this verifies that an inspection can be optimised using the superposition technique. This confirms that the superposition technique captures the necessary physics to simulate this data even at low SNR values. These results show an image amplitude error of 1.2 dB with the optimised filter averaged over 30 realisations of noise. While this error is larger than for the defects previously discussed, the standard deviation of the 30 realisations of the FE model was 1.3 dB and the individual images ranged from 11.6 to 17.8 dB above the RMS noise value meaning the error in the model is within the variation which can be expected in experimental samples.

V. Conclusion

The results have shown that the superposition technique described above gives accurate results for inspections where the SNR is such that defects are detectable without an unrealistically high false alarm ratio, including defects at the limit of what the inspection is capable of detecting. The technique begins to fail when the back wall signal becomes dominated by noise as it is then impossible to extract a reliable input signal for the analytical model. However, if this were the case in a real inspection, it is likely that ultrasonic imaging, at the given frequency, would not be the most appropriate

method of NDT. For the results presented here, this limit is reached at approximately 3.5 MHz, above this, the defect response shows a rapid reduction in accuracy as seen in figure 5, this coincides with the frequency at which the back wall amplitude drops below the +12.5 dB threshold shown in figure 6. in the images shown in figure 4D it is clear that there is no discernible back wall at frequencies at or above 3.5 MHz. The failure of the superposition technique at high frequency occurs due to the model taking its input signal from where the back wall should be present to simulate the defect and shadowing effects. However, the signal it captures is dominated by noise and so is unsuitable to be used as an input signal.

It has also been shown in table II, that while the individual speckle locations may vary in the image between the FE model and superposition model, the statistical properties of the noise have a negligible difference for the smaller defects considered and only a maximum of a 1.5 dB error for the largest defects. The back wall shadowing effects showed a larger error of approximately 4 dB for the 5 mm hole when filtered at a narrow bandwidth but when filtered using the optimised filter, this error is greatly reduced as seen in table II. The purpose of this technique is to aid in the simulation of defects close to the limit of detectability. For such defects, the model has been shown to give accurate predictions of defect amplitude, back wall shadowing and speckle statistics for defects with SNRs above the threshold level of 12.5 dB for all cases where the back wall signal in the defect free case is also above the 12.5 dB threshold. Thus, for the cases considered here, the fact that at high frequency the back-wall signal cannot be reliably extracted and used to generate an input signal for the superposition technique is not a limitation because in this regime the defects are undetectable anyway.

The work in [10] showed that the superposition modelling technique is capable of providing accurate simulations for back wall and defect image amplitudes at a single level of coherent noise. This paper extends that work to show that the model is valid over the full range of SNRs where meaningful data can be drawn from the image, in this paper, this was defined as defects with an SNR 12.5 dB above the RMS noise amplitude. In addition, it has shown that there is a negligable difference in the image speckle statistics when simulating cracks of 2 mm length and holes of 2 mm diameter and under (errors in the range of 0.07-0.52 dB) for the given inspection and a minor difference for 5 mm cracks and 5 mm holes (1.40 dB & 2.23 dB respectively).

References

[1] H. B. Huntington, "On ultrasonic scattering by polycrystals," *Journal of the Acoustical Society of America*, vol. 22, pp. 362–364, 1950.

[2] F. E. Stanke and G. Kino, "A unified theory for elastic wave propagation in polycrystalline materials," *The Journal of the Acoustical Society of America*, vol. 75, no. 3, pp. 665–681, 1984.

[3] W. P. Mason and H. J. McSkimin, "Energy losses of sound waves in metals due to scattering and diffusion," *Journal of Applied Physics*, vol. 19, pp. 940–946, 1948.

[4] W. D. Rummel, "Probability of detection as a quantitative measure of nondestructive testing end-to-end process capabilities," *Materials Evaluation*, vol. 56, no. 1, p. 29, 1998.

[5] C. Annis, L. Gandossi, and O. Martin, "Optimal sample size for probability of detection curves," *Nuclear Engineering and Design*, vol. 262, pp. 98–105, September 2013.

[6] J. S. Knopp, J. C. Aldrin, E. Lindgren, and C. Annis, "Investigation of a model-assisted approach to probability of detection evaluation," *Review of Progress In Quantitative Nondestructive Evaluation, Vols 26A and 26B*, vol. 894, pp. 1775–1782, 2007.

[7] T. Hasegawa and K. Yosioka, "Acoustic-radiation force on a solid elastic sphere," *The Journal of the Acoustical Society of America*, vol. 46, no. 5B, pp. 1139–1143, 1969.

[8] J. C. Bamber and R. J. Dickinson, "Ultrasonic b-scanning - a computer simulation," *Physics In Medicine and Biology*, vol. 25, pp. 463–479, 1980.

[9] J. Dobson and P. Cawley, "Independent component analysis for improved defect detection in guided wave monitoring," *Proceedings of the Ieee*, vol. 104, pp. 1620–1631, August 2016.

[10] H. A. Bloxham, A. Velichko, and P. D. Wilcox, "Combining simulated and experimental data to simulate ultrasonic array data from defects in materials with high structural noise," *Ieee Transactions On Ultrasonics Ferroelectrics and Frequency Control*, vol. 63, pp. 2198–2206, December 2016.

[11] W. Lord, R. Ludwig, and Z. You, "Developments in ultrasonic modeling with finite element analysis," *Journal of Nondestructive Evaluation*, vol. 9, pp. 129–143, sep 1990.

[12] F. Moser, L. J. Jacobs, and J. M. Qu, "Modeling elastic wave propagation in waveguides with the finite element method," *Ndt & E International*, vol. 32, pp. 225–234, June 1999.

[13] M. B. Drozdz, *Efficient finite element modelling of ultrasound waves in elastic media*. PhD thesis, Imperial College London, 2008.

[14] A. Van Pamel, G. Sha, S. I. Rokhlin, and M. J. S. Lowe, "Finite-element modelling of elastic wave propagation and scattering within heterogeneous media," *Proceedings of the Royal Society A-Mathematical Physical and Engineering Sciences*, vol. 473, January 2017.

[15] F. Aurenhammer, "Voronoi diagrams - a survey of a fundamental geometric data structure," *Computing Surveys*, vol. 23, pp. 345–405, September 1991.

[16] S. Ghosh, Z. Nowak, and K. Lee, "Tessellation-based computational methods for the characterization and analysis of heterogeneous microstructures," *Composites Science and Technology*, vol. 57, pp. 1187–1210, 1997.

[17] F. Kocks, C. Tomé, and H.-R. Wenk, *Texture and Anisotropy. Preferred Orientations in Polycrystals and Their Effect on Material Properties*. Cambridge University Press, 01 2000.

[18] G. Ghoshal and J. A. Turner, "Numerical model of longitudinal wave scattering in polycrystals," *Ieee Transactions On Ultrasonics Ferroelectrics and Frequency Control*, vol. 56, pp. 1419–1428, July 2009.

[19] P. Huthwaite, "Accelerated finite element elastodynamic simulations using the gpu," *Journal of Computational Physics*, vol. 257, pp. 687–707, January 2014.

[20] M. B. Drozdz, *Efficient finite element modelling of ultrasound waves in elastic media*. PhD thesis, Imperial College London, 2008.